Image Processing, Simulation and Performance Predictions for the MicroMak Star Tracker

Carl A. Nardell, Raytheon
James Wertz, Microcosm
Paul B. Hays, Michigan Aerospace Corp.

1. Abstract

The MicroMak device is a new, high-precision, very compact star sensor weighing less than 100 grams, with three independent 4-degree square fields of view[1]. The collection telescope is a Maksutov design that incorporates three telescopes into a single sensor head. The sensor is designed for star identification and spacecraft attitude determination with a device that offers unprecedented low cost, volume and mass. While star trackers have achieved sub-arcsecond accuracy by utilizing sophisticated algorithms and complex hardware, the MicroMak sensor must rely on fairly efficient algorithms that utilize data from only the image sensor. This paper will discuss the attitude determination algorithm as well as a complete end-to-end simulation of the system that was used to optimize the design and predict performance. This simulation accepts various star and sensor parameters as inputs, and generates error estimates of attitude of the sensor. The inputs include color temperatures and magnitudes of stars, focal length, receiver aperture, reflectivity curves of mirrors, modulation transfer function of the telescope system, vignetting effects, jittter characteristics, spacecraft spin rate and spin axis, detector pixel size, read noise, dark noise, sensor update rate, quantum efficiency as a function of wavelength, and detector fill factor. A complete forward model of the optical train has been built, and used with a maximum likelihood estimator to generate estimates of sensor attitude. A Monte Carlo algorithm was used to generate error distributions on the attitude error given the noise and distortions injected into the measurement.

2. Introduction

The MicroMak consists of three individual optical systems which share a common aperture. The three identical systems are tilted by 30 degrees with respect to the aperture's axis, and are arrayed at 120 degree intervals around that axis. This produces three views of the sky, at the system's three focal place arrays, which have orthogonal direction components to each other. The optical layout of single system and the three optical systems are shown together is shown Figure 1. Three identical imaging systems share a common aperture. The FPA's are arranged around the outside of the system, and their surfaces are normal to the incoming light.

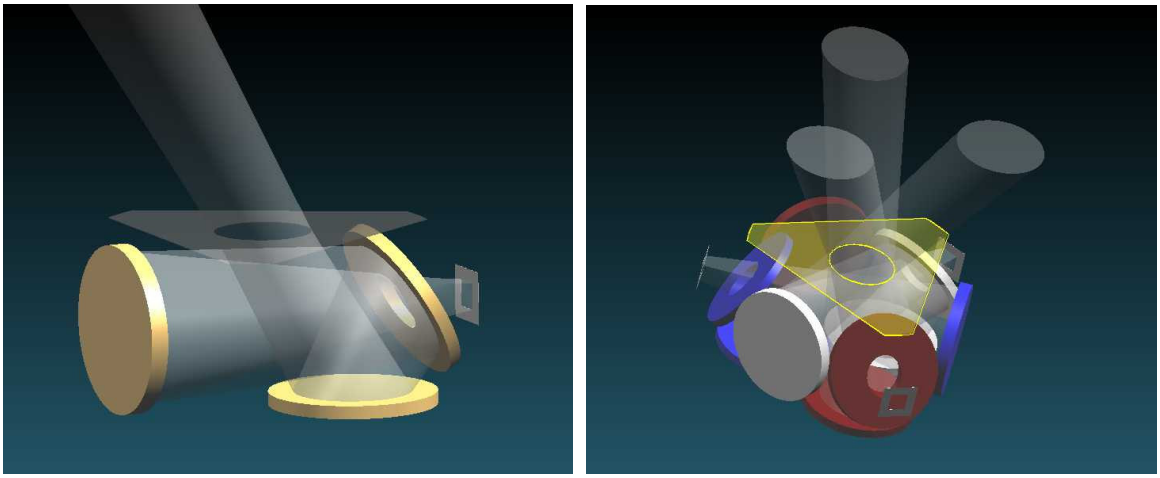

Figure 1: Left: Optical arrangement of a single system. Right: MicroMak with three fields of view through a common aperture.

The simulation effort presented herein has several motivations. The first is to develop and test attitude determination algorithms. While simple centroid determination algorithms are elegant and simple to implement, they are not sufficient when the spacecraft is spinning, or when low-frequency jitter is present. For this case, a more sophisticated estimation algorithm is required. Another motivation behind this effort is to provide a tool with which to optimize the optical design. Design decisions include selection of a focal plane array and geometry of the sensor, as there are presently dozens of possible choices for the focal plane array that include both CCD and CMOS devices. The third motivation for this work is to predict what performance can be expected of this device in terms of its ability to measure attitude for a given configuration in an absolute sense.

3. Description of Simulation

A complete end-to-end simulation of the system has been built. A schematic of this simulation is shown in Figure 2. The simulation accepts the following as inputs:

- Number of stars to use (up to 6)
- Whether or not to randomize the star inputs
- Color temperatures and magnitudes of stars (if not random)
- Focal length
- Receive aperture
- Reflectivity curve of mirrors
- Modulation transfer function of telescope system
- Vignetting
- Spacecraft spin rate and spin axis
- Detector pixel size
- Read noise
- Jitter frequency and magnitude or power spectral density (PSD)
- Charge transfer efficiency (CTE), where applicable
- Dark noise
- Update rate
- Quantum efficiency as a function of wavelength
- Fill factor

The simulation first generates a simulated detector image frame, and then estimates the position of the stars in the frame. The error is recorded and an attitude knowledge error is calculated. This process is repeated a specified number of times, and an error distribution results. This Monte Carlo approach is used to generate error distributions on the attitude error given the noise injected into the measurement; the image distortion resulting from spinning, and the effect of jitter on the sensor. The analytical calculation of this error estimate is difficult, particularly given the geometry of the star in the image plane when the spacecraft is rotating. While analytic estimates of the Cramer-Rao lower bound exist in the literaturei, they apply to the case of a purely Gaussian point spread function[2]. The simulation and Monte Carlo error analysis used herein is capable of utilizing an arbitrary point spread function, and includes the smearing effect of a spinning spacecraft.

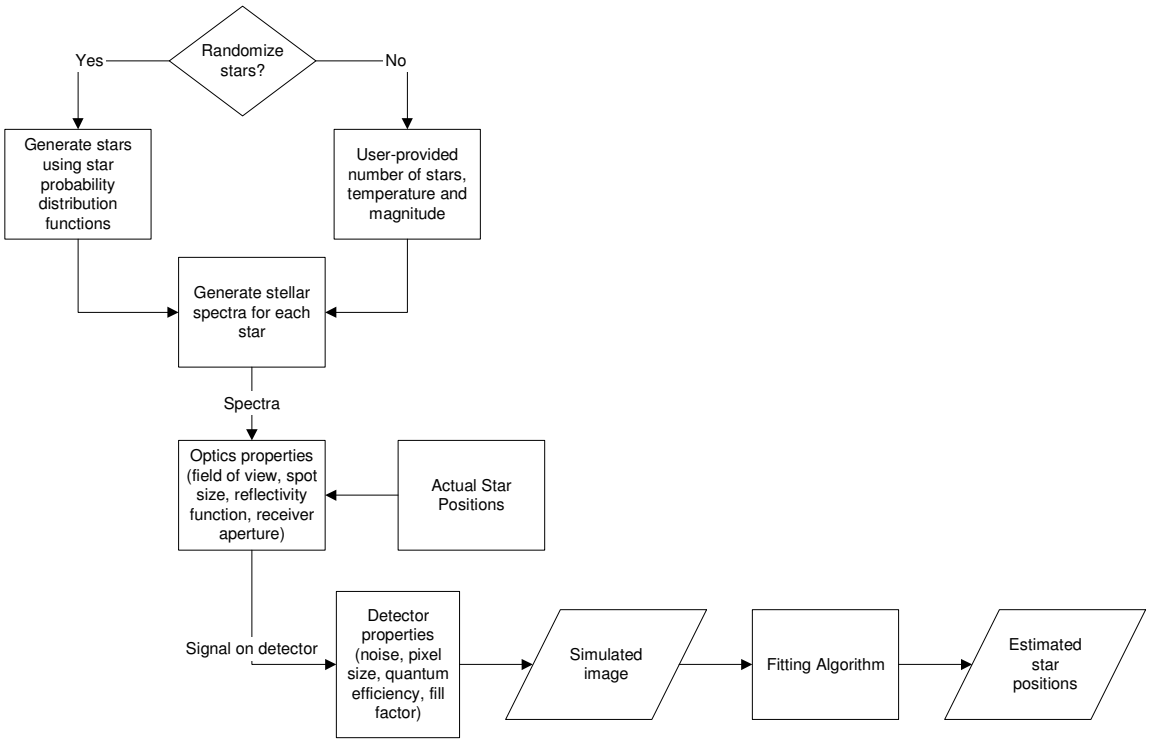

Figure 2: MicroMak forward model flow diagram

3.1. Star Sources and Detection Efficiency

The simulation first calculates star intensities as a function of wavelength. Once the star intensities have been calculated, the simulation calculates the detection efficiency of the detection system. The detector quantum efficiency as a function of wavelength is also used to calculate net detection efficiency for the incoming stellar radiation. The net signal from each star is calculated by the expression

$$B_i = \frac{\pi d^2 I_i p(1-v)}{4f} \qquad (1)$$

Where

d: telescope diameter
I_i: intensity of stars
p: pixel fill factor
v: vignetting as a percentage
f: readout rate in frames per second

This brightness is then used to calculate the intensity of a distributed point spread function in the image plane. The stars are assumed to be point sources, and the point spread function of the imager is assumed to be Gaussian. This is a reasonable assumption based on the ray trace and modulation transfer function analysis that was performed on the system. For a single star, the signal at any point in the image plane can be calculated by the expression

$$S(x, y, x_0, y_0) = B \frac{e^{\frac{-(x-x_0)^2-(y-y_0)^2}{2\sigma^2}}}{2\pi\sigma^2} \qquad (2)$$

Where x_o and y_o represent the coordinates of the centroid. The signal magnitudes calculated for the detected signal are then used to calculate a star image assuming random placement of the stars. The effect of overlap is another complication that is difficult to calculate analytically that is easily handled via the Monte Carlo method. A simulated image is shown in Figure 3.

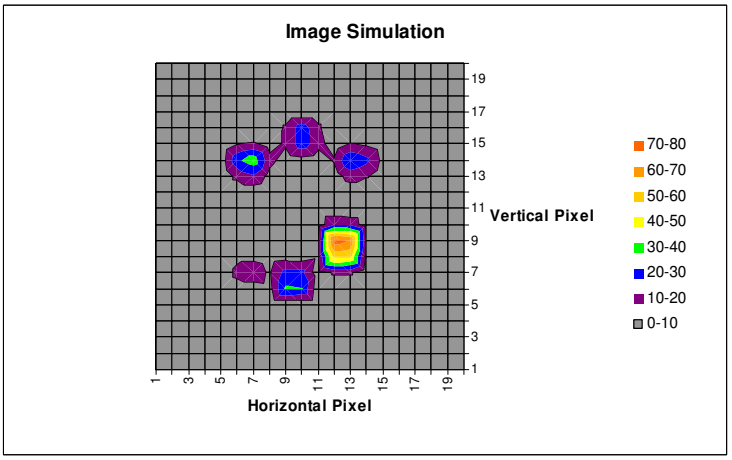

Figure 3: Simulated star image showing 6 stars of various color temperatures and visual magnitudes with no noise and zero spacecraft spin rate

When the spacecraft is rotating, or jitter is present, this distribution is distorted as a result of the motion of the source in the image plane during the integration period. The resulting image can be calculated by the expression

$$S'(x, y) = \int_{t=0}^{t_{\text{int}}} S(x, y, x_0 + v_x(t), y_0 + v_y(t))dt \qquad (3)$$

Where t_{int} is the inverse of the star tracker update rate, and vx and vy are the velocity of the tracker with respect to the scene in units of pixels per second. A sample image with a pure Gaussian point spread function is shown in Figure 4.

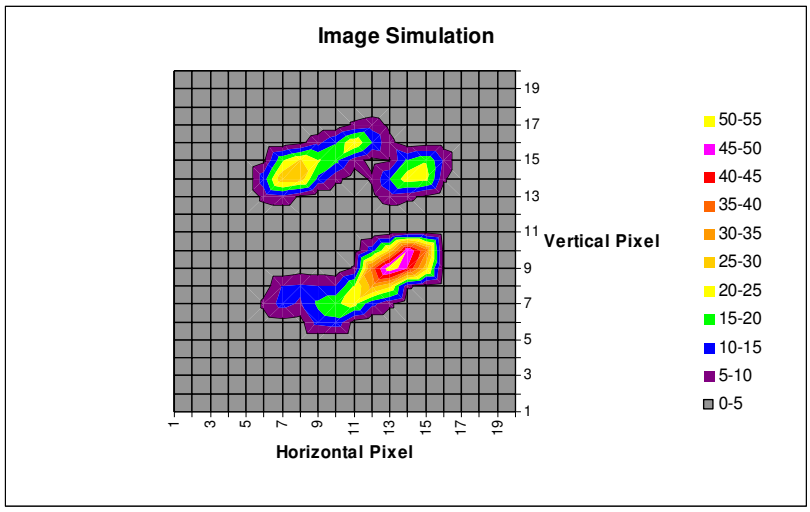

Figure 4: Simulated star image showing 6 stars with no noise and a spacecraft spin rate of .5 deg / sec

The image collected by the star tracker will be contaminated with read noise and dark noise. These are simulated and added to the simulated image. This is shown in Figure 5.

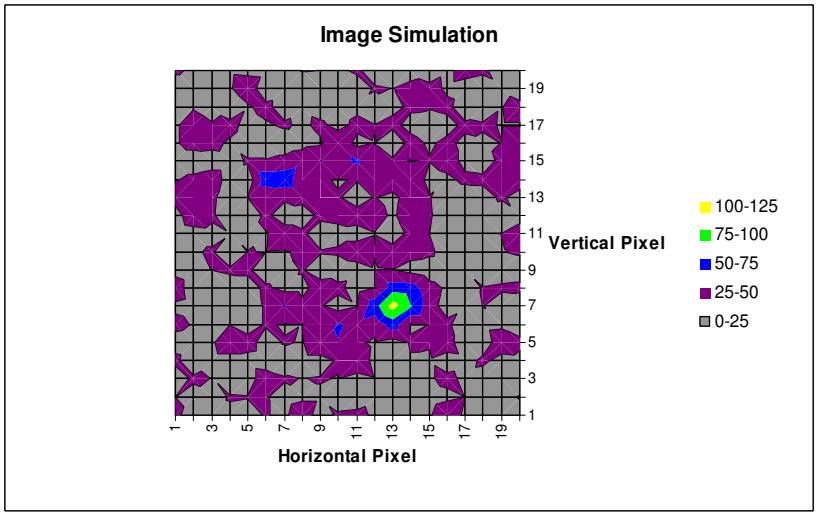

Figure 5: Simulated star image showing 6 stars with detector noise added

3.2. Simulation

One of the main functions of this simulation is to determine the measurement error for a given instrument configuration and design parameters. This is accomplished by development of the forward model presented in the earlier sections to generate a simulated image, and then using an estimation algorithm invert the image to provide star locations from the simulated data. The estimation algorithm makes use of the forward model, and adjusts the star locations in an effort to match the simulated noisy observation to the predicted image from the model. The estimation algorithm used here is the Levenberg-Marquardt non-linear inversion algorithm[3]. This technique is a maximum likelihood estimator whose behavior varies between an inverse-Hessian method and a steepest gradient decent method depending on the proximity to the solution. A top-level flow diagram of the simulation algorithm is shown in Figure 6.

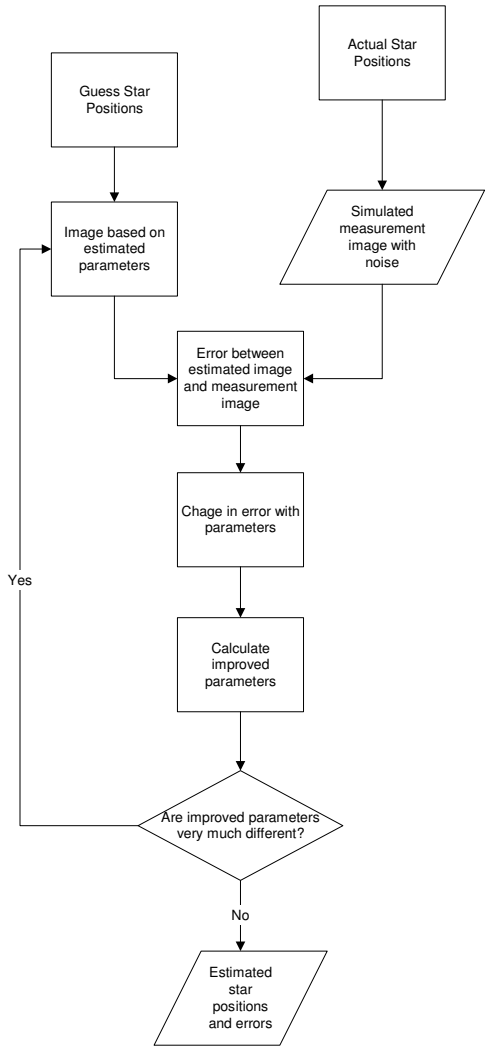

Figure 6: Estimation algorithm flow diagram

The fitting algorithm attempts to fit the x and y position of each of the stars in the simulation, as well as the velocity of the frame with respect to the scene. Rotation of the spacecraft will result in an elongation of the star image. This effect changes the ability of the system to measure star positions. The theoretical calculation of the measurement uncertainties is cumbersome as a result of the fact that the point spread function becomes a piecewise function when the spacecraft is spinning. For the purpose of parameter estimation, the forward model is calculated using an analytic expression for the point spread function elongation that results from rotation of the spacecraft instead of calculating the integral shown in Eq. 3. For this simulation, the simple Gaussian point spread function is smeared in one direction as a result of the spinning motion. The length, l, in units of detector pixels, of the smear is calculated by

$$l = \frac{\omega N}{2\theta f} \tag{4}$$

where ω is the rotation rate of the spacecraft (rad / sec); N is the number of detector pixels across the field of view; θ is the field of view (rad); and f is the update rate of the sensor, or the inverse of the integration time in seconds. Calculation of this effect in the image plane involves a coordinate system rotation and translation. For a given point, x, y, in the detector plane, The signal, $S(x,y)$ is given by

$$S(x,y)=\begin{cases}\dfrac{e^{\frac{-x''^2-y''^2}{2\sigma^2}}}{2\pi\sigma^2}, & x''<0\\ \dfrac{e^{\frac{-(x''-l)^2-y''^2}{2\sigma^2}}}{2\pi\sigma^2}, & x>l\\ \dfrac{e^{\frac{-y''^2}{2\sigma^2}}}{2\pi\sigma^2}, & \text{O.W.}\end{cases} \tag{5}$$

where

$$\begin{aligned} x'' &= x' - \Delta x \\ y'' &= y' - \Delta y \end{aligned} \tag{6}$$

$$\begin{aligned} x' &= R\cos\left[\tan^{-1}\left(\frac{y}{x}\right)-\phi\right] \\ y' &= R\sin\left[\tan^{-1}\left(\frac{y}{x}\right)-\phi\right] \end{aligned} \tag{7}$$

$$\Delta x = \sqrt{\frac{x_0^2+y_0^2}{1+\tan^2\left[\tan^{-1}\left(\frac{y_0}{x_0}\right)-\phi\right]}} \tag{8}$$

$$\Delta y = \sqrt{\frac{x_0^2+y_0^2}{1+\frac{1}{\tan^2\left[\tan^{-1}\left(\frac{y_0}{x_0}\right)-\phi\right]}}}$$

ϕ is the direction of the axis of rotation in the coordinate frame of the detector, and x_0, y_0 are the coordinates of the center of the star at the beginning of the integration period. It is assumed that the optical performance (σ, point spread function) of the sensor is well-know, and is not a fit parameter. This results in a maximum 3x3 inversion. In principle, the spin direction can be fit as well, but the inversion becomes nearly singular at low SNR, particularly at low spin rates where the image is nearly symmetrical in any spin direction. This simulation uses a single value decomposition for matrix inversion in the interest of robustness. It was assumed that knowledge of spin direction is available from another on-board system, and that this information will be provided to the star tracker. It might also be possible to obtain spin direction from successive estimates of attitude and performing time derivatives in an effort to estimate the rotation vector, but this has not been investigated in this study.

In practice, the initial guess is generated by using a random number generator to generate an initial parameter vector specifying star positions that is perturbed from the actual by some unknown amount. The estimation algorithm is then used on many data frames to generate distributions of the errors. The average error over many runs represents the

expected variance of the measurement. This Monte Carlo technique can be used to estimate absolute and relative errors for various instrument parameters and states.

While the practice of generating a complete forward model and inverting it is unlikely to be implemented in an operational system due to computational expense, it can be considered a lower limit on the measurement error that is possible with other algorithms. Concepts involving geometric centroid calculation, using prior estimates to generate a new one (Kalman filtering), lookup tables, and digital filtering are all likely to be utilized in practice. The errors from these methods are likely to be similar, or perhaps somewhat greater than the full non-linear inversion employed in this analysis.

3.3. Jitter

When a star tracker is located on a spacecraft in a location that is in close proximity to a vibration source, or when it is located on a structure that exhibits flexure, jitter will impact the accuracy of attitude measurements. This is a function of both jitter amplitude and frequency. Jitter may be in the form of a sinusoidal oscillation, such as what might be seen at the end of a boom or in the form of random vibration, which may be encountered in close proximity to complex mechanisms, such as refrigerators or rotating scanners.

Two types of jitter were simulated for this effort. Sinusoidal oscillation was considered in two directions: parallel and perpendicular to the spacecraft spin axis. This was simply modeled as a sinusoidal variation of the center of the image spot. Random jitter was also modeled. While each spacecraft will exhibit its own unique jitter frequency spectrum, a spectrum was used that it fairly typical of medium-size space structures with a jitter input.[4] Random vibration inputs were generated by generating a sequence of displacements having a uniform power spectrum, and then filtering that series with an infinite impulse response (IIR) filter having the desired spectral characteristics. The IIR filter was designed using the Yule-Walker method[5], which allows specification of a power spectral density (PSD) profile, and uses a time-domain least squares fitting approach to calculate filter coefficients. The PSD profile used is a fairly simple low-pass filter that can be realized with a relatively low-order filter. A 10-order filter was used for an optimal balance between computational expense and spectral fidelity. A pole-zero plot of the filter is shown in Figure 7, and the filter response is shown in Figure 8.

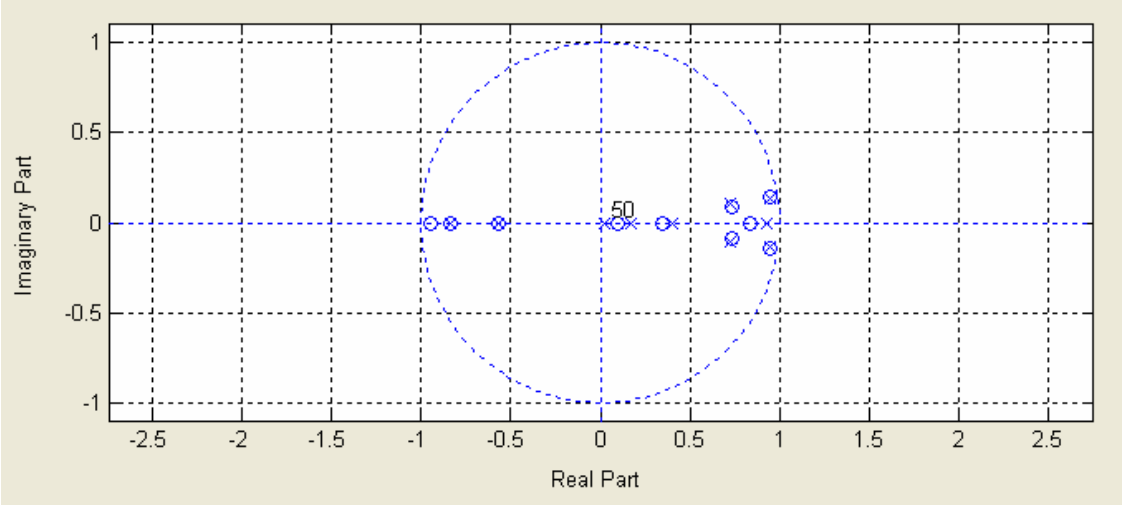

Figure 7: Pole-zero plot of the filter used to generate random vibration.

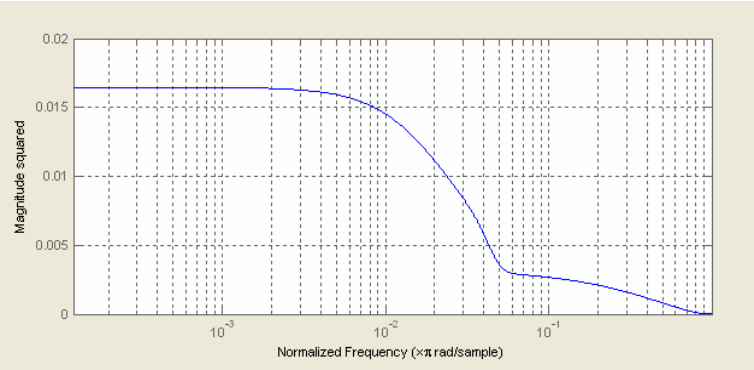

Figure 8: Frequency response of the filter used to generate random vibration

4. Results

Results of the simulations are presented in two parts. First, generic optimizations are presented for the design parameters without regard to the particular design elements of the MicroMak. The second part of the results apply these generic optimizations to the MicroMak, and result in performance predictions of the sensor.

4.1. Optimizations

A series of Monte Carlo simulations were run to determine optimal system parameters for a generic imaging system with a given signal available, noise level, rate of rotation, pixel size and image size. In the results that follow, signal-to-noise ratio is defined as the ratio of the total signal from the source to the signal due to noise sources in each pixel. This includes read and dark current sources, and is assumed to be normally distributed. The questions that are of most importance in the hardware design are primarily what is required with regard to clear aperture, pixel size and focal length.

Figure 9 (left) shows the effect of image blur or pixel size and noise on the accuracy of the position estimate. Image blur is defined as 1/e encircled energy of the Gaussian point spread function. An optimal value of the ratio of pixel size to image blur is approximately 2:1. This result depends slightly on the noise level present. Figure 9 (right) shows the dependency of position estimate on the rotation velocity of the spacecraft. As expected, as the sensor begins to rotate, image smear degrades the ability to accurately measure position. The effect of spin rate on the expected error is one of the more difficult to calculate analytically, and the one that has been addressed in the literature the least.

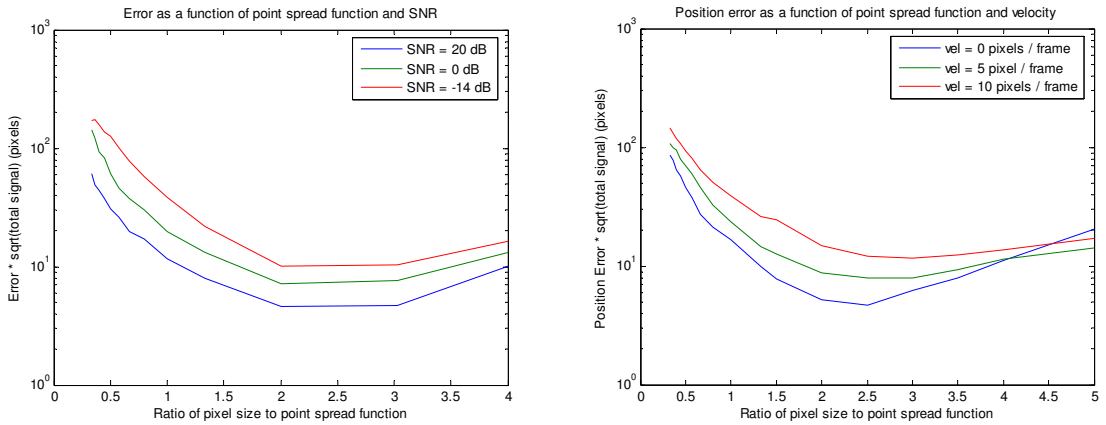

Figure 9: Left: Position error as a function of pixel size and SNR for a single star. Right: Position error as a function of pixel size and rotational velocity.

Figure 10 shows the relationship between position measurement accuracy and jitter frequency and amplitude for oscillation normal and parallel to the spin axis of the spacecraft. For these cases, sinusoidal jitter is introduced to the image. The effect of jitter parallel to the spin axis has a more negative impact on position estimation. This is due to the fact that in the case of jitter normal to the spacecraft axis, the algorithm treats the jitter as a rotational velocity. This is particularly true at low frequencies.

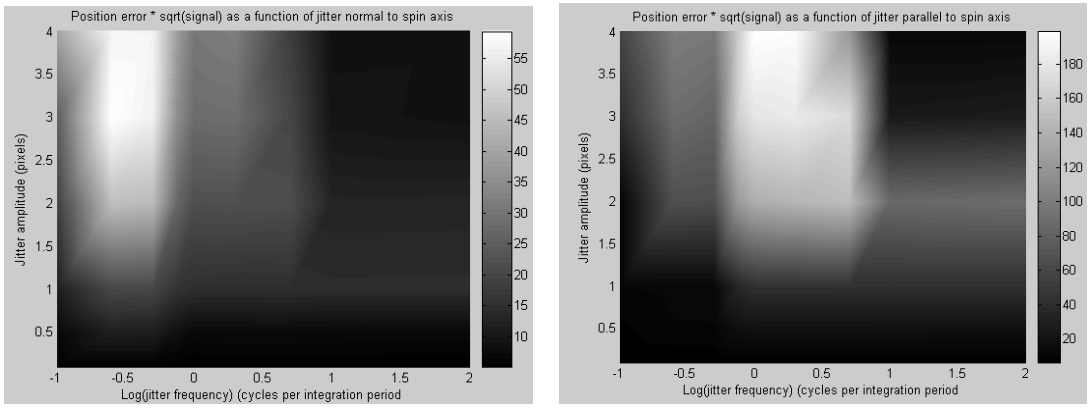

Figure 10: Position error for a single star as a function of jitter amplitude and frequency for jitter that is normal (left) and parallel (right) to the spacecraft spin axis.

For the case of random two-dimensional vibration, the impact on position error is shown in Figure 11. As would be expected, the sensor is most intolerant of low-frequency, large amplitude oscillations, as these induce a bias. As frequency increases, the effect of jitter becomes more analogous to a larger image blur, which does not introduce an asymmetric image degradation. This result implies that if jitter is expected, it will impact the choice of the pixel size, as a larger pixel size would be preferable in the presence of jitter.

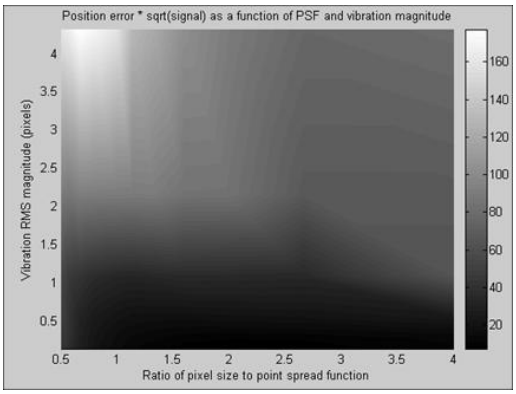

Figure 11: Position error for a single star as a function of pixel size and vibration magnitude

4.2. Performance Predictions

Once generic optimizations were completed, the models were used to predict sensor performance for various configurations being considered. For all of the cases presented, three stars were used with the following properties:

Star #	Visual Magnitude	Color Temperature
1	7	17000
2	7	4000
3	7	11000

The other nominal instrument parameters were

Parameter	Nominal value
Pixel width	12 microns
Dark noise	3 e- / sec
Read noise	20 e- / read
Detector CTE	.99995
Fill factor	90%
Telescope diam.	.55 cm
Read rate	10 Hz
Point spread function	12 microns FWHM
Focal length	4.32 cm
Vignetting	50%
Spin rate	0 deg. / sec.
Spin direction	0 deg.
Jitter	None

The first parameter that was studied was the relationship between error and telescope diameter. We would expect the variance to be a function of the diameter squared, since the photon counting process can be modeled as a Poisson process. A power fit to the data shows an exponent of 2.02, which is very close to the expected theoretical behavior for a Poisson process. This is shown in Figure 12. The effect of velocity on this sensor is shown in Figure 13. Figure 14 shows the variation in position error as a function of pixel size and noise level.

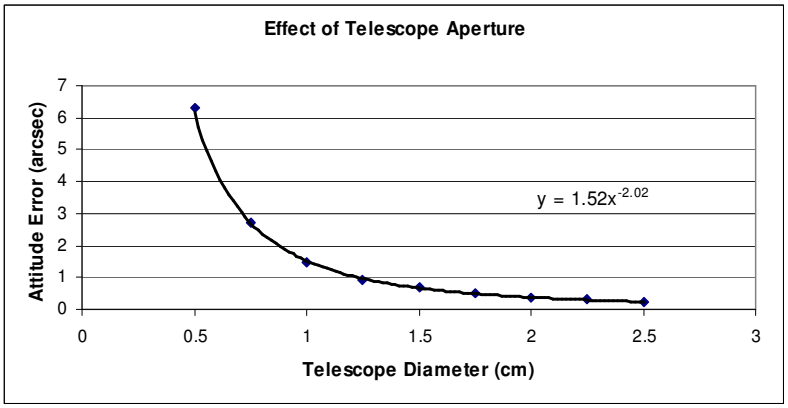

Figure 12: Effect of telescope aperture on measurement accuracy for the case of 3 magnitude-7 stars

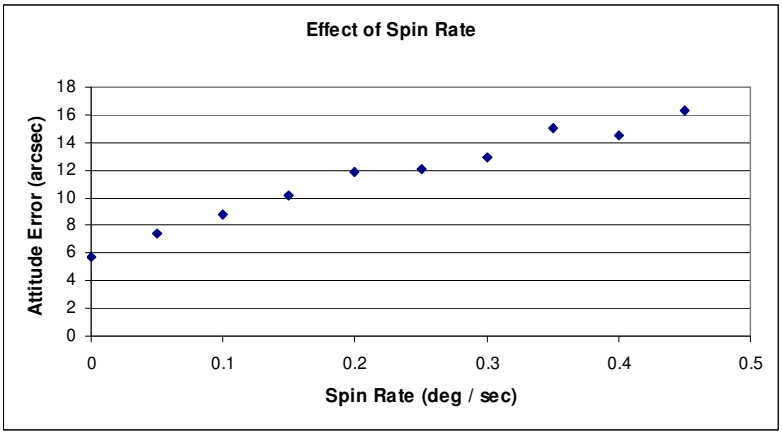

Figure 13: Effect of spacecraft spin rate on measurement accuracy for the case of 3 magnitude-7 stars

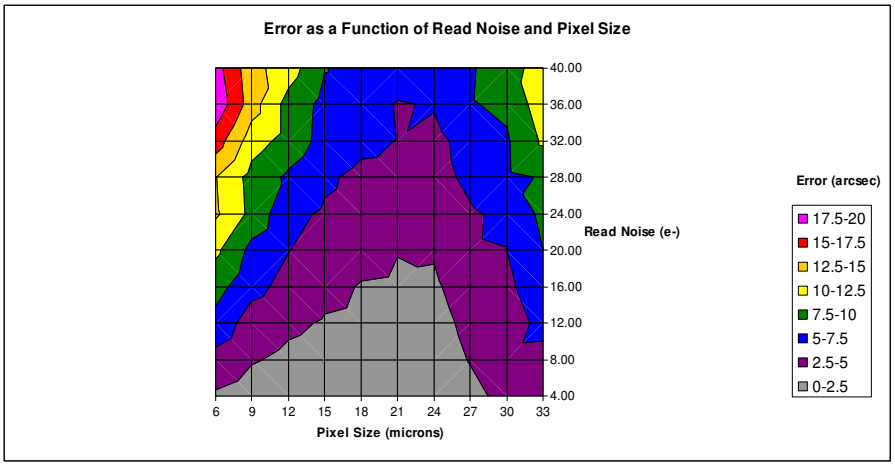

Figure 14: Effect of pixel size and read noise on measurement accuracy for the case of 3 magnitude-7 stars. This case was generated for a 12-micron point spread function.

5. Summary and conclusions

The results presented here show the approximate position measurement accuracy that can be expected for an imaging system that measures star positions in the presence of jitter and image smear due to movement during signal integration. These results provide guidelines for the optimization of sensors such as the MicroMak star tracker. These results also show that the MicroMak sensor is capable of achieving arc-second accuracy if a detector with adequately low read noise can be implemented.

---

[1] U.S. Patent #6,060,072.

[2] Winick, K.A. "Cramer-Rao lower bounds on the performance of charge-coupled-device optical position estimators," J. Opt. Soc. Am. A, Nov. 1986, p. 1809 – 1815

[3] Press, W.H., Teukolsky, S.A., Vetterling, W.T., Flannery, B.P., Numerical Recipes in C, Cambridge University Press, 1994, pp. 683.

[4] Gupta, A., et al., "Attitude determination for high-accuracy submicroradian jitter pointing on space-based platforms," *Proc. SPIE* **1303**, 1990, p. 336 – 349.

[5] Friedlander, B., and B. Porat, "The Modified Yule-Walker Method of ARMA Spectral Estimation," IEEE Transactions on Aerospace Electronic Systems, AES-20, No. 2, March 1984, p. 158-173.